

# Origins of Peptide Selectivity and Phosphoinositide Binding Revealed by Structures of Disabled-1 PTB Domain Complexes

Peggy C. Stolt,<sup>1,4</sup> Hyesung Jeon,<sup>1,4</sup> Hyun Kyu Song,<sup>2</sup> Joachim Herz,<sup>3</sup> Michael J. Eck,<sup>2</sup> and Stephen C. Blacklow<sup>1,\*</sup>

<sup>1</sup>Department of Pathology  
Brigham and Women's Hospital and  
Harvard Medical School  
75 Francis Street  
Boston, Massachusetts 02115

<sup>2</sup>Department of Cancer Biology  
Dana Farber Cancer Institute and  
Department of Biological Chemistry  
and Molecular Pharmacology  
Harvard Medical School  
44 Binney Street  
Boston, Massachusetts 02115

<sup>3</sup>Department of Molecular Genetics  
University of Texas Southwestern Medical Center  
Dallas, Texas 75390

## Summary

Formation of the mammalian six-layered neocortex depends on a signaling pathway that involves Reelin, the very low-density lipoprotein receptor, the apolipoprotein E receptor-2 (ApoER2), and the adaptor protein Disabled-1 (Dab1). The 1.5 Å crystal structure of a complex between the Dab1 phosphotyrosine binding (PTB) domain and a 14-residue peptide from the ApoER2 tail explains the unusual preference of Dab1 for unphosphorylated tyrosine within the NPxY motif of the peptide. Crystals of the complex soaked with the phosphoinositide PI-4,5P<sub>2</sub> (PI) show that PI binds to conserved basic residues on the PTB domain opposite the peptide binding groove. This finding explains how the Dab1 PTB domain can simultaneously bind PI and the ApoER2 tail. Recruitment of the Dab1 PTB domain to PI-rich regions of the plasma membrane may facilitate association with the Reelin receptor cytoplasmic tails to transduce a critical positional cue to migrating neurons.

## Introduction

The mammalian Disabled-1 (Dab1) gene is one of two known mammalian orthologs of *Drosophila* Disabled, a gene required for proper development of the fly central nervous system [1, 2]. Genetic and biochemical studies of Dab1 in mice and in humans have shown that it is required for the migration of neurons to their proper positions during embryonic development. Targeted or naturally occurring disruption of Dab1 in mice causes abnormal neuronal positioning in the cerebral cortex and the hippocampus, as well as cerebellar dysplasia [3, 4].

The Dab1 null phenotype is identical to that of the

ataxic *reeler* mouse, which results from a naturally occurring null mutation in the *reelin* gene [5]. The connection between Reelin, a secreted protein found in the extracellular matrix, and Dab1, a cytosolic adaptor protein, was revealed when double-knockout mice lacking two closely related proteins of the low-density lipoprotein (LDL) receptor gene family, ApoER2 and VLDLR, were shown to be phenotypically indistinguishable from *reeler*- and *dab1*-deficient mice [6]. Studies showing that Reelin binds to the ectodomains of ApoER2 and VLDLR [7, 8] and that Dab1 binds to the cytoplasmic tails of these receptors [9] provide further compelling evidence that Reelin, the lipoprotein receptors, and Dab1 are part of a common signaling pathway.

A phosphotyrosine binding (PTB) domain at the N terminus of Dab1 mediates binding to the cytoplasmic tails of the lipoprotein receptors [9, 10]. This domain is required for normal Dab1 function and is shared among the three known isoforms of Dab1 [11]. All isoforms also include a tyrosine-rich sequence immediately C-terminal to the PTB domain, with variations resulting from alternative splicing occurring downstream (Figure 1A).

Though PTB is an acronym for “phosphotyrosine binding” [12–14], PTB domains exhibit remarkable plasticity in their ability to recognize different peptide motifs. In Dab1, the PTB domain selectively recognizes peptides with the consensus sequence  $\phi$ xNPxY (where  $\phi$  represents F or Y, x represents relaxed amino acid selectivity, and Y is designated the “0” position on the basis of prior convention). In contrast to most other PTB domains that bind tyrosine-based motifs either with preference for phosphotyrosine (at the 0 position) or indifference to the phosphorylation state of the tyrosine, the PTB domain of Dab1 favors unphosphorylated tyrosine over phosphotyrosine by almost two orders of magnitude [15]. In accordance with this observed selectivity, the tyrosine of the NPxY motif of each receptor is believed to be unphosphorylated at rest, and whether receptor activity is regulated by phosphorylation on the NPxY tyrosine is not yet known.

PTB domains structurally resemble pleckstrin homology (PH) domains, which bind to a variety of different phospholipids with varying specificity [16–18]. Indeed, previous studies have shown that the Dab1 PTB domain binds phosphoinositides (PIs) [15], with selectivity for phosphatidylinositol-4,5-bisphosphate (PI-4,5P<sub>2</sub>), although the significance of PI-4,5P<sub>2</sub> binding by Dab1 has not yet been elucidated. Binding of PI-4,5P<sub>2</sub> can occur in the absence of peptide and does not prevent peptide binding in competition experiments, suggesting the existence of a distinct PI-4,5P<sub>2</sub> binding site [15]. The other mammalian homolog of *Drosophila* Dab, Dab2, which seems to participate in mediating endocytosis of different LDL receptor-related proteins, also selectively binds PI-4,5P<sub>2</sub> at a site that does not prevent peptide binding [19], suggesting that a distinct PI binding site has been

\*Correspondence: sblacklow@rics.bwh.harvard.edu

<sup>4</sup>These authors contributed equally to this work.

Key words: ApoER2; Disabled; lipoprotein receptor; phosphoinositide; Reelin signaling; X-ray crystallography

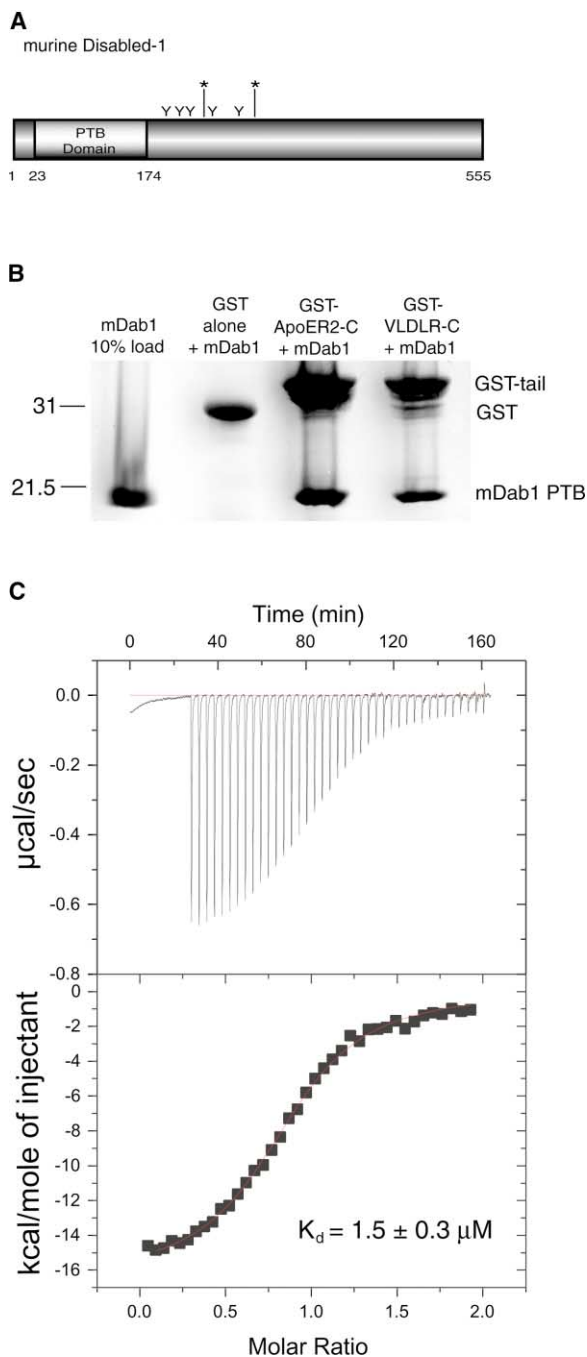


**Figure 1. Dab1 Domain Organization, Formation of PTB-ApoER2 Peptide Complexes, and Measurement of Affinity**

(A) Schematic diagram of Dab1. The five regulatory tyrosines downstream of the PTB domain are indicated, and sites of alternative splicing are marked with an asterisk.

(B) GST pull-down of the Dab1 PTB domain by the ApoER2 and VLDLR cytoplasmic domains (ApoER2-C and VLDLR-C). Bound protein was subjected to SDS-PAGE and visualized by staining with Coomassie blue.

(C) Measurement of the dissociation constant of the complex between the Dab1 PTB domain and a 14-residue peptide from the ApoER2 tail by isothermal titration calorimetry (ITC). A stock solution of the peptide (170  $\mu\text{M}$ ) was added in 7.5  $\mu\text{l}$  increments into a 20  $\mu\text{M}$  solution of the Dab1 PTB domain. To calculate the dissociation constant, we fitted data to a one-site binding model with the program Origin 5.0.

evolutionarily conserved in these two related proteins, which exhibit  $\sim 60\%$  identity in their PTB domains.

To understand the basis for selective recognition of peptides with an unphosphorylated tyrosine at the 0 position, we determined the structure of the Dab1 PTB domain in complex with a 14-residue peptide from the ApoER2 cytoplasmic tail. The structure of the complex, determined at 1.5  $\text{\AA}$  resolution, indicates how this PTB domain selectively binds peptides with the  $\phi\text{xNPxY}$  consensus sequence and why unphosphorylated tyrosine is preferred. The structure of the PTB domain-peptide complex also reveals the presence of a basic patch on the surface of the PTB domain on the face opposite the peptide binding groove; by soaking PTB-peptide cocrystals in  $\text{PI-4,5P}_2$ , we also determined the site of  $\text{PI-4,5P}_2$  binding within this patch in a ternary complex.

## Results and Discussion

Primary sequence alignment and secondary structure prediction indicated that the region of homology between Dab1 and known PTB domains extends from residue 23 to 174. The construct chosen for production of the Dab1 PTB domain in bacteria spanned residues 20–175 (Dab1 PTB domain hereafter) to ensure inclusion of the entire domain with minimal flexibility at either terminus (Figure 1A).

Because this Dab1 PTB domain polypeptide differs at both termini from other previously studied Dab1 constructs [9, 15], we first verified that our purified Dab1 PTB domain associates with peptides derived from the cytoplasmic tails of ApoER2 and VLDLR in a pull-down assay. When glutathione beads are loaded with GST fusion proteins displaying either the ApoER2 or VLDLR peptide, the Dab1 PTB domain is indeed recovered with the beads, whereas it is not pulled down by GST alone (Figure 1B).

The dissociation constants of different Dab1 PTB domain-peptide complexes were then measured directly by isothermal titration calorimetry (ITC) and/or fluorescence polarization. The  $K_d$  of the complex between the ApoER2 14-mer ( $\text{Ac-TKSMNFDNPVYRKT-CONH}_2$ ) and the PTB domain, measured by ITC, is  $1.5 \pm 0.3 \mu\text{M}$  (Figure 1C), an affinity comparable to that previously measured by fluorescence for binding of a 17-residue APP peptide to a different Dab1 PTB domain-GST fusion construct [15] and within the range seen for complexes of peptides with PTB domains from other proteins [20–22]. Further analysis of the ITC data indicates that the binding of the ApoER2 peptide is enthalpy driven, as seen for the binding of peptides to the PTB domains of IRS1 and SNT-1 [21, 23] and in contrast to binding of peptides to the Shc PTB domain [23]. Competition binding experiments by fluorescence polarization show that a 10-mer ApoER2 peptide, from which the four N-terminal residues have been deleted, binds the PTB domain of Dab1 with an affinity indistinguishable from that of the 14-mer ApoER2 peptide (data not shown).

## Crystallization and Overview of Structure

To understand the basis for recognition of the 14-mer by the Dab1 PTB domain, we solved the crystal structure

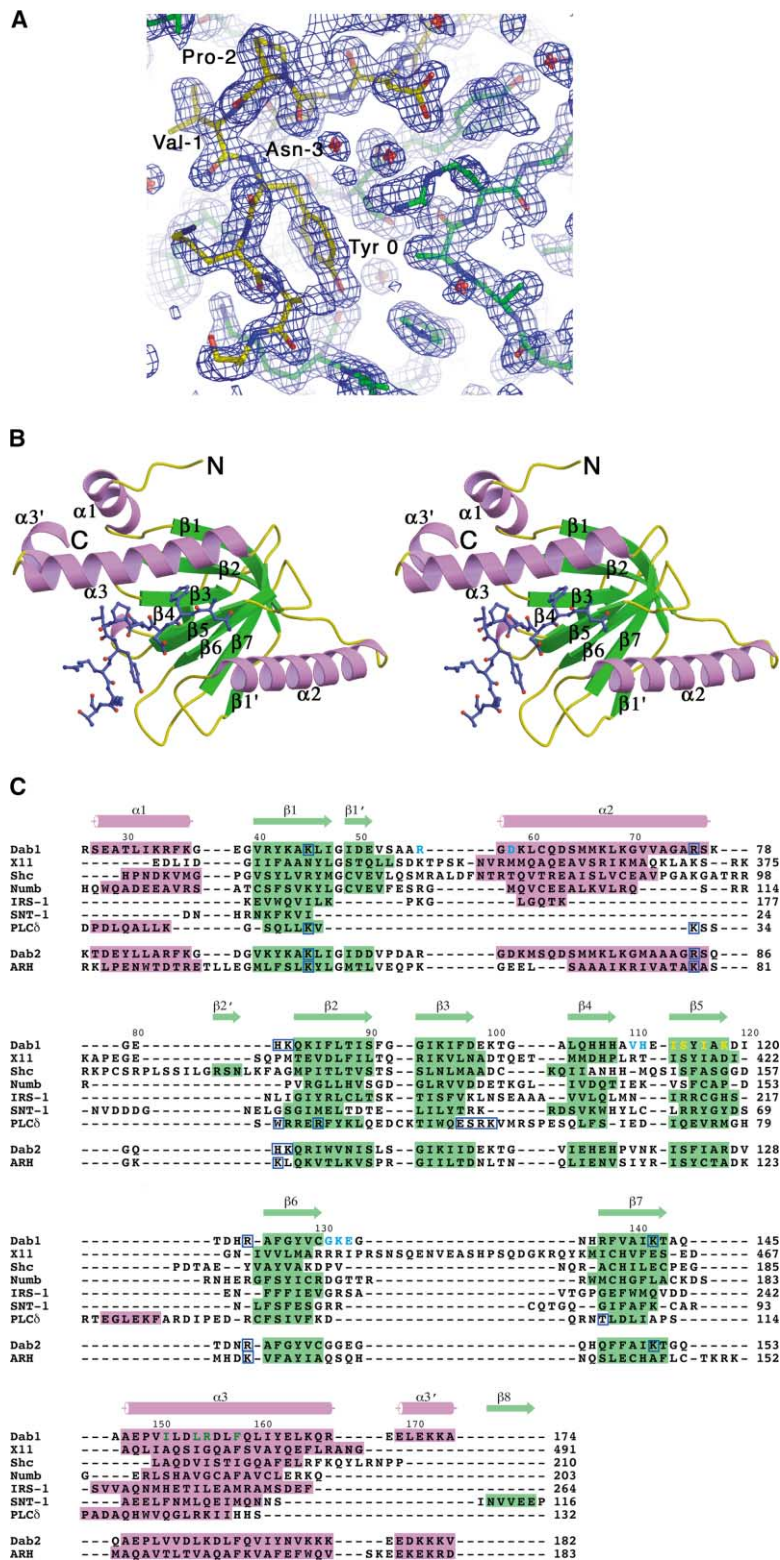


Figure 2. Electron Density, Overview of Structure, and Sequence Alignment

(A) Representative electron density (contoured at  $1\sigma$  after refinement) from the residues surrounding the NPVY motif of the peptide in the Dab1 PTB domain-peptide complex. Peptide residues, yellow; protein residues, green.

(B) Ribbon representation of the Dab1 PTB domain in stereo colored according to secondary structure, with bound peptide rendered in ball and stick form.

(C) Structure-based alignment of the Dab1 PTB domain with other PTB domains and a representative PH domain. Secondary structure elements are colored as in (B). Residues in the Dab1 PTB domain that interact with the ApoER2 peptide are colored cyan (hydrogen bonds), green (hydrophobic interactions), or yellow (both). Residues of the Dab1 PTB domain and the PLC $\delta$  PH domain that contact PI-4,5P $_2$  are enclosed in blue boxes, as are the aligned residues of the Dab2 and ARH sequences. Numbers above the alignment refer to residue positions in Dab1. Residue positions for the other proteins are shown to the right of the aligned sequences.

of this complex by multiwavelength anomalous dispersion (MAD) to 1.5 Å resolution (Figure 2A; Table 1). The phase information was derived from selenomethionine-substituted Dab1 harboring an L87M mutation because the two consecutive native methionines of the Dab1 PTB

domain (M65 and M66) alone failed to provide enough phasing power to solve the structure.

The Dab1 PTB domain exhibits a canonical PTB fold, in which seven central  $\beta$  strands form two antiparallel, near-orthogonal  $\beta$  sheets, capped by a long C-terminal

Table 1. Crystallographic Data Collection and Refinement

	L87M (MAD)				
	Native	Remote	Peak	Edge	PI-4,5P <sub>2</sub> Soaked
<b>Data Collection</b>					
Wavelength (Å)	0.909	0.95004	0.97815	0.97872	1.5418
Resolution (Å)	1.5	1.9	2.0	2.0	1.9
(outer shell) <sup>a</sup>	(1.5–1.54)	(1.9–1.98)	(2.0–2.07)	(2.0–2.07)	(1.9–1.96)
Total reflections	141,192	71,181	128,475	128,909	34,852
Unique reflections	24,532	11,465	10,278	10,309	12,179
Completeness (%) <sup>a</sup>	99.5 (98.9)	94.1 (68.9)	96.9 (81.1)	96.9 (80.9)	98.0 (97.5)
R <sub>merge</sub> (%) <sup>a,b</sup>	5.2 (23.5)	4.2 (13.6)	4.9 (9.0)	4.1 (9.4)	4.7 (17.0)
Figure of merit (before/ after DM) <sup>c</sup>			0.779 / 0.852		
<b>Refinement</b>					
Resolution range (Å)	40–1.5				40–1.9
Number of reflections	24,472				11,884
R <sub>work</sub> /R <sub>free</sub> (%) <sup>d</sup>	0.222/0.245				0.204/0.253
Number of atoms (main chain/side chain/all chains, residues)					
mDab1	609/592/1201, 23–174				609/592/1201, 23–174
Peptide	41/48/89, 5–14				41/48/89, 5–14
Water	160				151
PO <sub>4</sub> or PI-4,5P <sub>2</sub>	5				48
Average B value (Å <sup>2</sup> ) (main chain/side chain/all chains)					
mDab1	15.16/19.44/17.27				21.38/25.44/23.38
Peptide	20.30/23.13/21.82				28.52/31.39/30.09
Water	28.76				36.96
PO <sub>4</sub> or PI-4,5P <sub>2</sub>	33.73				40.57
Rms bond length (Å)	0.004				0.005
Rms bond angles (°)	1.12				1.08

<sup>a</sup> Values in parentheses are for reflections in the highest resolution bin.

<sup>b</sup>  $R_{\text{merge}} = \sum_i \sum_j |I_{h,j} - \langle I_h \rangle| / \sum_i \sum_j I_{h,j}$ , where  $I_{h,j}$  is the intensity of the  $j^{\text{th}}$  measurement of  $h$  and  $\langle I_h \rangle$  is the corresponding average value for all  $i$  measurements.

<sup>c</sup> Figure of merit =  $|\sum P(\alpha) e^{i\alpha} / \sum P(\alpha)|$ , where  $P(\alpha)$  is the phase probability distribution and  $\alpha$  is the phase.

<sup>d</sup>  $R_{\text{work}}$  and  $R_{\text{free}} = \sum ||F_o| - |F_c|| / \sum |F_o|$  for the working set and test set (10%) of reflections.

$\alpha$  helix (Figure 2B). Even though all PTB domains for which structures have been solved share a low level of sequence identity, structure-based alignment reveals that this core topological framework is universally conserved (Figure 2C). Unique insertions building upon this framework are occasionally found; the Dab1 PTB domain, like the PTB domains of Shc, X11, and Numb [20, 24, 25], contains an insertion between strands  $\beta 1$  and  $\beta 2$  that forms an extra  $\beta$  strand as well as a long  $\alpha$  helix (Figures 2B and 2C). The PTB domain of Dab1 includes a short N-terminal  $\alpha$  helix also seen in the corresponding regions of the Shc and Numb PTB domains.

### Peptide Conformation

The Dab1 PTB domain binds the ApoER2 peptide in a hydrophobic groove formed by the  $\beta 5$  strand and the C-terminal helix in a mode like that seen in the Shc-, IRS-1-, X11-, and Numb-peptide complexes [20, 22, 24, 26]. In the Dab1-peptide complex, the four N-terminal residues of the peptide (positions –7 to –10; Figure 3A) are disordered, explaining why a 10-mer lacking these residues has comparable affinity for the Dab1 PTB domain. Asn –6 to Asp –4 of the peptide adopt an extended conformation, forming backbone hydrogen bonds with residues in the  $\beta 5$  strand to add another strand to the C-terminal  $\beta$  sheet of the PTB domain; the adjacent NPxY motif forms a type I  $\beta$  turn (Figures 3A

and 3B). These global conformational features of the bound peptide are also seen in most other structures of peptides bound to PTB domains.

The Dab1 PTB domain contacts the side chains of the bound peptide at a number of sites (Figures 3A and 3B). Phe –5 of the peptide packs tightly into a hydrophobic groove created by Ile151, Leu154, the aliphatic part of Arg155, and Phe158 of the C-terminal  $\alpha$  helix, explaining the preference for Phe or Tyr at this position [15]. The carboxylate of the adjacent Asp at –4 forms a saltbridge with the guanidino group of Arg56. The Asn of the NPVY sequence forms two H bonds between the hydrogen atoms of its NH<sub>2</sub> group and main chain carbonyl oxygens of Val110 and Ile113 of the PTB domain. The side chain carbonyl oxygen of this Asn residue in the Dab1-peptide complex also participates in an intrapeptide H bond with the Val –1 backbone amide to initiate the  $\beta$  turn formed by the NPxY motif. In the structures of peptides bound to other PTB domains, the corresponding Asn residues form similar hydrogen bonds, and the presence of this Asn is vital for peptide recognition [20, 26]. The type I  $\beta$  turn of the NPVY sequence positions the Tyr 0 residue in a cleft formed by His111, Glu112, and Ser114, enabling formation of an H bond between the Tyr 0 side chain OH and the backbone carbonyl of Gly131 (Figures 3A and 4A).

The conformation of the polypeptide backbone from

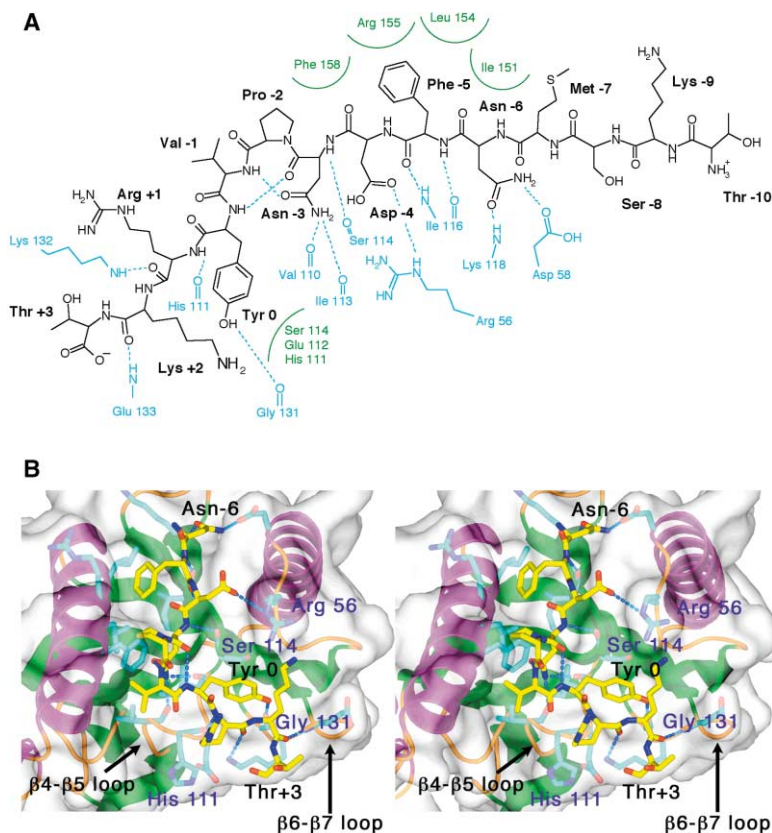


Figure 3. Dab1 PTB Domain-Peptide Contacts

(A) ApoER2 peptide sequence with schematic indicating contacts between the peptide and the Dab1 PTB domain. Hydrogen bonds, dotted cyan lines; hydrophobic contacts, green. (B) Stereo representation of contacts. For the peptide, side chains are yellow, and residue labels are black. For the PTB domain, side chains are cyan, and residue labels are purple. A transparent surface of the PTB domain is shown in white, and the PTB domain backbone is illustrated with ribbons. Hydrogen bonds, dashed blue lines.

Asn - 6 to Tyr 0 of the central NPxY sequence is nearly identical to that of the corresponding region of the APP peptide bound to the X11 PTB domain [20]. The APP peptide in its conformation from the X11 cocrystal structure readily superimposes onto the ApoER2 peptide bound to Dab1 (Figure 4A, top panel). This superposition shows that the PTB domain of Dab1 can accommodate the APP peptide with Tyr 0 in a similar position and without steric clashes elsewhere, consistent with the known ability of an overlapping APP peptide to bind to the PTB domain of Dab1 with low micromolar affinity [15].

A distinct feature of the Dab1 PTB domain is its strong preference for unphosphorylated Tyr at the 0 position. This discrimination highlights a key difference between Dab1 and X11 because X11 does not readily distinguish between Tyr and pTyr [20]. Selection against pTyr by Dab1 is established by a cleft created by the short loops connecting  $\beta 4$  with  $\beta 5$  and  $\beta 6$  with  $\beta 7$  (Figures 3B and 4A), which closely approach the tyrosine side chain and should sterically exclude the bulkier pTyr. This cleft is capped at one end by the loop connecting  $\beta 1$  with the central helix. The tight turn connecting strands  $\beta 6$  and  $\beta 7$  of the mDab1 PTB domain packs against this cap. This arrangement results in an H bond between the tyrosine hydroxyl and the backbone carbonyl of Gly131 (Figures 3 and 4A, bottom panel) and also places the His136 imidazole ring within van der Waals contact of the tyrosine hydroxyl. The presence of this H bond also explains the observed strong preference for Tyr over Phe at the 0 position [15].

In contrast, the corresponding loop connecting  $\beta 6$

with  $\beta 7$  is different in other PTB domains of known structure (Figure 2C). In particular, the same loop in X11 is much longer and disordered in the crystal, and the  $\beta 6$  strand in X11 does not extend as far toward the Tyr of the peptide. The mobility of these loops may enable X11 to bind both Tyr and pTyr sequences, while the limited flexibility of the short loops combined with the closer approach of the  $\beta 6$  strand in Dab1 only accommodates Tyr (Figures 3B and 4A). Whereas the long  $\alpha 2$  helix of Dab1 packs against the  $\beta 1'$ ,  $\beta 6$ , and  $\beta 7$  strands, holding the  $\beta 6$ - $\beta 7$  loop in place and constraining the Tyr 0 binding pocket, IRS-1 lacks  $\beta 1'$  and the long  $\alpha 2$  helix and instead features a much shorter helix that connects strands  $\beta 1$  and  $\beta 2$ , but does not approach the Tyr 0 binding pocket, allowing adequate space for the phosphate group (Figure 4B, top panel). Finally, the  $\beta 6$ - $\beta 7$  loop of IRS-1 also contains a bulge imposed by a GPG sequence (residues 232-234) at its C-terminal end [26]. The two glycine residues of the GPG bulge make backbone H bonds to residues on either side of Arg227, and the proline buttresses the aliphatic part of the Arg 227 side chain. These interactions situate Arg227 in position to form a salt bridge with the pTyr phosphate group and, together with Arg 212, create the positively charged pocket dictating the preference for pTyr in IRS-1 (Figure 4B).

Of note, a homology model of a complex between the ICAP-1 $\alpha$  PTB domain and a  $\beta 1$  integrin peptide also predicts that this PTB domain should prefer to bind peptides with unphosphorylated Tyr within the NPxY motif. In that model, which is of high structural quality

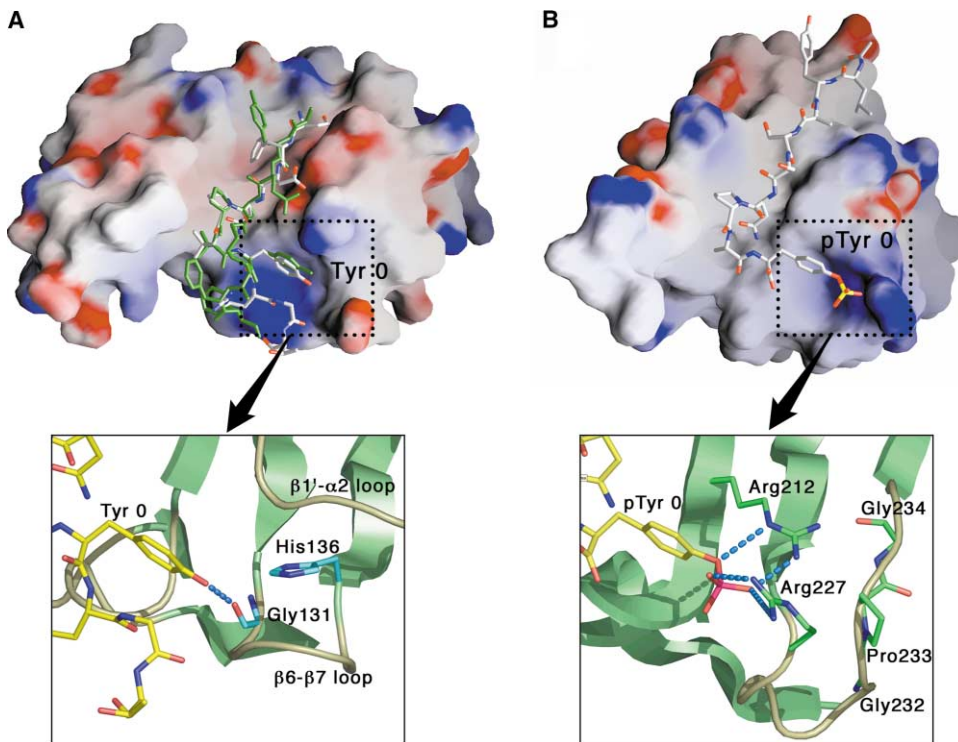


Figure 4. Comparison of the Dab1 PTB Domain-ApoER2 Complex with Other PTB Complexes

(A) Top panel, superposition of the APP peptide onto the Dab1 PTB domain-ApoER2 peptide complex. The molecular surface representation of the Dab1 PTB domain is colored by electrostatic potential ( $-15$  kt/e [red] to  $+15$  kt/e [blue]). The ApoER2 (gray) and APP (green) peptides are rendered in stick form, and the lysine side chain of the ApoER2 peptide has been removed for clarity. Bottom panel, close-up view of the boxed region highlighting the residues interacting with the Tyr 0 residue of the ApoER2 peptide. The protein backbone is shown as a ribbon, while selected peptide (yellow) and protein (cyan) side chains are in stick form. Hydrogen bonds, dashed blue lines.

(B) The IRS-1 PTB domain-pTyr peptide complex. Top panel, the molecular surface representation of the IRS-1 PTB domain [26] is colored by electrostatic potential (as in [A]) to illustrate the basic pocket responsible for phosphotyrosine binding. The bound insulin receptor peptide is rendered in stick form. Bottom panel, close-up view of the boxed region to highlight the residues interacting with the pTyr of the insulin receptor peptide. Colored as in (A), except that the protein side chains are green.

and has a backbone rmsd of  $1.05 \text{ \AA}$  to our X-ray structure for all alignable residues (460 atoms), the ICAP-1 $\alpha$  PTB domain also has a short loop connecting  $\beta 4$  with  $\beta 5$ , and the  $\beta 6$ - $\beta 7$  loop is predicted to project an Ile side chain toward the Tyr of the peptide, thereby discriminating between Tyr and pTyr [27].

#### A Mechanism for Membrane Recruitment

The selective binding of PI-4,5P $_2$  by both Dab1 and Dab2 may direct recruitment of these proteins to the membrane [15, 19]. PI-4,5P $_2$  binding may control mechanisms of transport of Dab family proteins within cells and/or their localization within specific membrane compartments, like lipid rafts. In addition, in ways not yet understood, PI-4,5P $_2$  binding may also participate in integrating the binding of the ApoER2 cytoplasmic tail with other events in signaling, for example, by facilitating kinase-catalyzed tyrosine phosphorylation of Dab1 or by coupling of the receptor-Dab1 complex to downstream signaling pathways [28, 29].

How does Dab1 bind PI-4,5P $_2$ ? The structure of the PTB domain-peptide complex reveals a distinct region of positive electrostatic surface potential on the surface of the PTB domain opposite the peptide binding groove. This patch results from a coalescence of basic side

chains derived from the residues in the loops connecting adjacent secondary structural elements. To test whether this basic patch encompasses the PI-4,5P $_2$  binding site and concurrently determine how PI-4,5P $_2$  binds to the PTB domain, we soaked PTB-peptide cocrystals in mother liquor containing PI-4,5P $_2$ .

Crystals soaked with PI-4,5P $_2$  show strong density for the phosphates in the 4 and 5 positions, with additional contiguous density from the inositol ring and 1-phosphate groups. The observed density is best modeled by the binding of PI-4,5P $_2$  in either of two orientations (see Experimental Procedures), which are related to each other by a  $180^\circ$  rotation around an axis bisecting the 4- and 5-phosphate groups and perpendicular to the C4-C5 bond of the inositol ring (Figure 5). The primary difference between these two orientations is defined by the position of the 1-phosphate group because PI-4,5P $_2$  is pseudosymmetric around the rotation axis. The preferred conformation (by a 70:30 ratio, as estimated by occupancy refinement; see Experimental Procedures) situates the 1-phosphate close to Arg76, and we therefore discuss interactions of the PI-4,5P $_2$  with the PTB domain using that orientation.

In this model, the phosphates of PI-4,5P $_2$  interact with six of the residues that make up the conserved basic

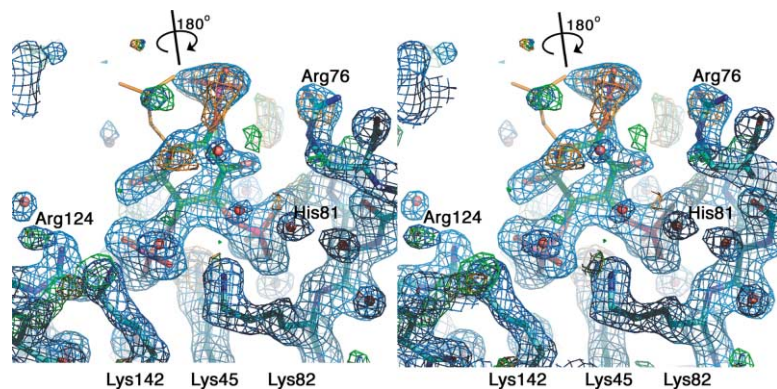


Figure 5. Electron Density of PI-4,5P<sub>2</sub> Bound to the Dab1 PTB Domain  
Bound PI-4,5P<sub>2</sub> was modeled in two orientations related by a 180° axis of rotation. PI-4,5P<sub>2</sub> in the preferred orientation, based on occupancy refinement (see Experimental Procedures), CPK colors; the orientation with the lower occupancy, orange. Orange mesh, F<sub>o</sub> - F<sub>c</sub> map after refinement of a model with PI-4,5P<sub>2</sub> in the less occupied orientation, contoured at 2.5 σ. Note the large regions of residual electron density overlapping the positions of the 1-phosphate and the 2-hydroxyl in the preferred orientation. Green mesh, F<sub>o</sub> - F<sub>c</sub> map after refinement of a model with PI-4,5P<sub>2</sub> in the preferred orientation, contoured at 2.5 σ. Note the residual region of electron density overlapping the position of the 1-phosphate in the other orientation. Blue mesh, 2F<sub>o</sub> - F<sub>c</sub> map, contoured at 1 σ, of a composite model including refined coordinates of both PI-4,5P<sub>2</sub> orientations weighted by occupancy. Protein side chains interacting with bound PI-4,5P<sub>2</sub> are indicated.

region on the Dab1 PTB domain surface (Figures 2C and 5). Two 4-phosphate oxygens are coordinated by the guanidino group of Arg124 from the N-terminal end of β6 and the ε-amino group of Lys142 from the C-terminal end of β7. His81 coordinates one of the 5-phosphate oxygen atoms, and the ε-amino groups of Lys45 and Lys82 are in position to coordinate terminal oxygen atoms from both the 4- and 5-phosphates. The side chain of Arg76 is also close enough to the 1-phos-

phate of the preferred orientation to form a salt bridge to one of the terminal oxygen atoms (Figure 5).

The residues that comprise the phosphoinositide binding site are conserved among a subset of PTB domain-containing proteins homologous to Dab1 (Figure 6). All of the residues that contact PI-4,5P<sub>2</sub> are strictly conserved in the sequence of Dab2, which also binds PI-4,5P<sub>2</sub> and otherwise harbors only ~60% identity to Dab1 in its PTB domain [30]. A Dab1-based homology

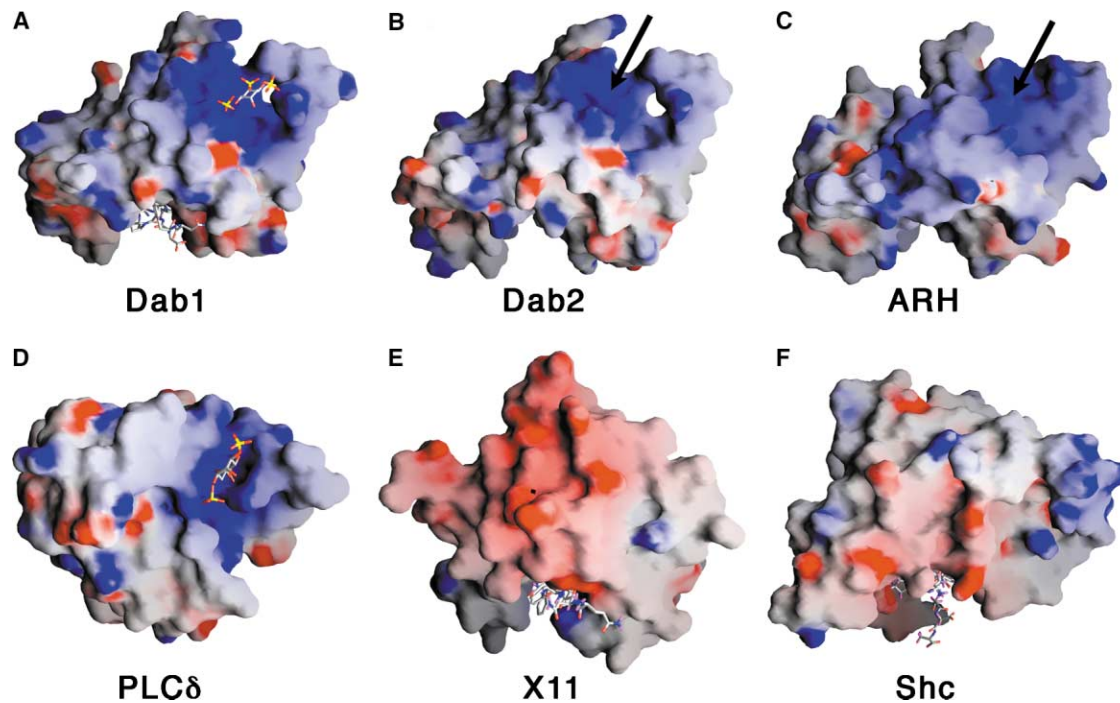


Figure 6. The PI-4,5P<sub>2</sub> Binding Site Is Shared by Dab1, Dab2, and PLCδ, but Not by X11 and Shc

(A) The Dab1 PTB domain, oriented with the peptide binding groove at the base and the N-terminal residues of the bound peptide projecting toward the viewer. The PI-4,5P<sub>2</sub> binding site is on the top face, opposite the peptide binding groove. Dab1-based homology models of the Dab2 (B) and the ARH (C) PTB domains show that the location of the positively charged PI-4,5P<sub>2</sub> binding site is conserved (arrows). (D) The PH domain from PLCδ bound to PI-4,5P<sub>2</sub> [33]. The basic residues that form the PI-4,5P<sub>2</sub> binding site in PLCδ structurally align with the amino acids that create the PI-4,5P<sub>2</sub> binding site in Dab1. The X11 (E) and Shc (F) PTB domains lack the basic residues that make up the PI-4,5P<sub>2</sub> binding site. All molecular surface representations were generated by the program GRASP [46] and shaded by electrostatic potential (-15 kt/e [red] to +15 kt/e [blue]).

model of the Dab2 PTB domain also predicts the presence of a comparable basic region at the same location (Figure 6B), further suggesting that the conservation of the basic patch is important for the function of both proteins. In addition, these basic residues are also conserved in the ARH protein (Figure 2C), another PTB domain-containing protein that shares the ability to bind both the cytoplasmic tails of LDL receptor family members and PI-4,5P<sub>2</sub> [31, 32]. A homology model of ARH based on the Dab1 structure shows that these residues would similarly form a basic PI binding surface (Figure 6C), suggesting that membrane recruitment may be a general feature of interactions between LDL receptor family members and their adaptor proteins. Finally, the PI-4,5P<sub>2</sub> binding site of a representative PH domain, the one from phospholipase C $\delta$ , [33] consists of basic residues in loops connecting secondary structural elements, which also align structurally with the residues used by Dab1 (Figures 2C and 6D), suggesting a potential evolutionary relationship between Dab1 and the PI binding PH domains.

The basic patch is a distinguishing feature of the Dab1-like subset of PTB domains because the corresponding residues are not conserved in other PTB domains of known structure, like those of the X11 and Shc proteins (Figures 6E and 6F). In such proteins, there may either be no need for membrane recruitment (although the Shc PTB domain may bind weakly to PI-4P and PI-4,5P<sub>2</sub> at a site that appears to compete with peptide binding using residues distinct from the ones identified here [24, 34, 35]) or this function may be fulfilled by another domain of the protein. For example, in IRS-1, an adjacent PH domain binds to PIs to bring IRS-1 to the membrane [36].

The PTB domain of Dab1 combines the peptide binding features of typical PTB domains with the PI binding properties characteristic of most PH domains (Figure 7). This combination of membrane recruitment and peptide binding by a single domain suggests that these activities are functionally coupled. Membrane recruitment of the Dab1 PTB domain by the basic region may help to orient the ligand binding groove with respect to the ApoER2 peptide, which lies only  $\sim 10$  residues from the trans-membrane sequence. Selectivity of the PTB domain for PI-4,5P<sub>2</sub> may serve to concentrate the Dab1 signaling complex in membrane patches that are highly enriched in this phospholipid, thus facilitating coupling to, and activation of, PI-3 Kinase, a component of a downstream branch of the Reelin signaling pathway [28].

### Biological Implications

Control of neuronal migration during development depends on a signaling pathway that includes the secreted protein Reelin, the ApoER2 and VLDLR cell surface receptors, and the adaptor protein Dab1. Dab1 binds to an NPxY-containing motif in the cytoplasmic tails of ApoER2 and VLDLR via its N-terminal PTB domain. Both Dab-1 and the related protein Dab-2 also bind PI-4,5P<sub>2</sub>, suggesting that the activity of Dab-1 may also depend on or be regulated by recruitment to PI-enriched membrane compartments.

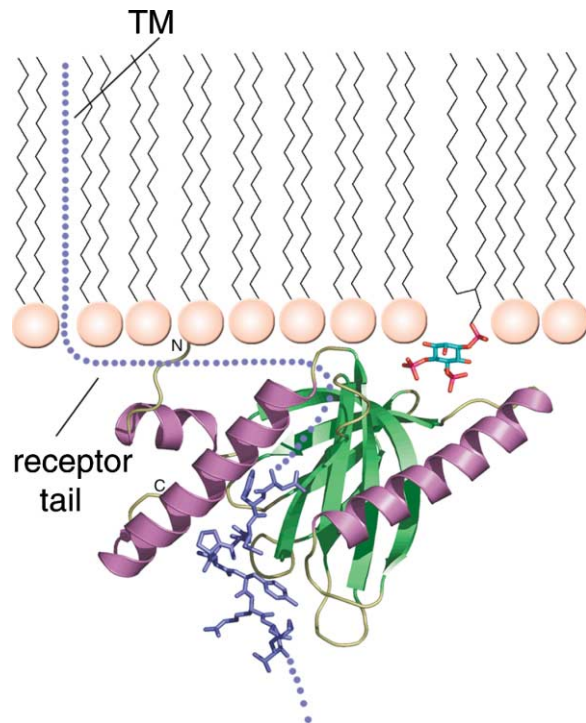


Figure 7. A Model for the Arrangement of the Dab1-ApoER2 Complex at the Membrane Surface

Structure of the ternary complex of the Dab1 PTB domain (ribbon trace, colored as in Figure 2A), ApoER2 peptide (blue sticks), and PI(4,5)P<sub>2</sub> (cyan- and CPK-colored sticks), arranged to illustrate that membrane recruitment of the PTB domain by PI(4,5)P<sub>2</sub> is fully compatible with binding to the ApoER2 cytoplasmic tail. The positions of the remainder of the ApoER2 receptor cytoplasmic tail (blue dots) and the phospholipid membrane are highly schematized in the model.

To understand the basis for selective recognition of peptides with an unphosphorylated tyrosine at the 0 position and to identify potential sites for PI binding, we determined the structure of the Dab1 PTB domain in complex with a 14-residue peptide from the ApoER2 cytoplasmic tail. The structure of the Dab1 PTB domain-peptide complex explains why the Dab1 PTB domain strongly prefers peptide ligands in which the Tyr of the NPxY motif is not phosphorylated. Although it is not known whether the NPxY motif of either lipoprotein receptor tail undergoes phosphorylation, the preference for unphosphorylated tyrosine shows that it would be possible to regulate downstream signaling by modulating the tyrosine phosphorylation state of the receptor tails.

In the ternary complex of the Dab1 PTB domain, peptide, and PI-4,5P<sub>2</sub>, the PI-4,5P<sub>2</sub> binds to the large basic patch on the face of Dab1 opposite the peptide binding groove. These studies provide the first structural characterization of a hybrid PTB domain to which both peptide and PI-4,5P<sub>2</sub> have been simultaneously bound and provide support for models in which Dab1 function is enabled or regulated by PI binding. Control of membrane localization by PI binding may regulate Dab1 activity by facilitating downstream events that accompany peptide binding, such as tyrosine phosphorylation by mem-

brane-associated kinases. In addition, the ability of Dab1 to bind to PIs may itself be diminished when the tyrosine residues adjacent to the PTB domain are phosphorylated upon activation of a Reelin signal [7, 37, 38]. Insights from our structures of Dab1 PTB-ApoER2 peptide complexes should open up several new lines of investigation to clarify the role of PI binding by Dab1 in living cells.

## Experimental Procedures

### Subcloning, Protein Expression, and Purification of the Dab1 PTB Domain

The sequence encoding the PTB domain of Dab1 (residues 20–175) was amplified by PCR from a full-length cDNA clone (kindly provided by Brian Howell). The PCR product was introduced into the pDEST15 vector downstream of glutathione S-transferase (GST) without the use of restriction sites by recombinational Gateway cloning (Invitrogen); a tobacco etch virus (TEV) protease cleavage site was introduced between GST and the Dab1 PTB domain during subcloning. The L87M mutation, which enabled incorporation of selenomethionine into the protein for structure determination by MAD, was carried out by PCR mutagenesis with a QuickChange site-directed mutagenesis kit (Stratagene). Native and selenomethionine-labeled fusion proteins were expressed in *E. coli* BL21(DE3) and in *E. coli* B834(DE3) methionine-auxotrophic cells, respectively, by induction with IPTG (0.4 mM). For purification of native and selenomethionine-labeled proteins, cells were lysed either by sonication or with a French press in 20 mM Na<sub>2</sub>HPO<sub>4</sub> buffer (pH 6.8) containing 150 mM NaCl, 20% sucrose, 1 mM EDTA, 5–10 mM DTT, 200 μM PMSF, 1 μg/ml aprotinin, and 0.5 μg/ml leupeptin (buffer A). After each GST-Dab1 fusion protein was captured on glutathione-Sepharose beads (Pharmacia), the PTB domain was released from bound GST by cleavage with His<sub>6</sub>-tagged TEV protease. After removal of TEV protease from solution with Ni-NTA agarose (Qiagen), the native and selenomethionine-labeled proteins were then purified to apparent homogeneity by anion exchange followed by gel filtration chromatography. For crystallography, purified proteins were concentrated and dialyzed into 50 mM Tris buffer (pH 6.8) containing 50 mM NaCl and 5 mM DTT. For binding studies and biophysical measurements, the protein was dialyzed exhaustively against a solution of 10 mM Na<sub>2</sub>HPO<sub>4</sub> buffer (pH 6.8) containing 150 mM NaCl and 5 mM DTT.

### GST Pull-Down

The cytoplasmic tails of ApoER2 (ApoER2-C) and VLDLR (VLDLR-C) were expressed as GST fusion proteins with a modified version of the pGEX-4T-1 vector (Pharmacia) that harbors a TEV protease site before the polylinker. The GST-fusion proteins, as well as GST alone, were expressed in *E. coli* BL21(DE3) cells by induction with IPTG. Cells were lysed by sonication in buffer A. The lysates were gently agitated together with glutathione-Sepharose beads (Pharmacia) to permit binding of the GST fusion proteins. After three washes with 10 mM Na<sub>2</sub>HPO<sub>4</sub> (pH 7.5), 150 mM NaCl, 5 mM DTT, and 0.5% NP-40 (buffer B), glutathione-Sepharose beads loaded either with GST-ApoER2-C, GST-VLDLR-C, or GST alone (10 μl) were gently rocked in the presence of the purified Dab1 PTB domain (10 μM) in buffer B (1.0 ml) for 2 hr at 4°C. The beads were recovered by centrifugation, washed three times in buffer A (1 ml), and resuspended in 50 μl of SDS-PAGE loading buffer. After boiling for 10 min, bound proteins were separated by SDS-PAGE with a 15% gel and were visualized by staining with 0.1% Coomassie brilliant blue.

### Binding Measurements

The affinities of the purified Dab1 PTB domain for 10- and 14-residue Apo-ER2 tail peptides were measured by isothermal titration calorimetry (ITC) and/or by fluorescence polarization. For ITC measurements, a 14-residue synthetic peptide from the ApoER2 cytoplasmic tail (Research Genetics; acetyl-TKSMNFDNPVYRKT-amide) was purified by reversed-phase HPLC for titration into a solution of the Dab1 PTB domain. A stock solution of the tail peptide (170 μM) was added in 7.5 μl increments to a 20 μM solution of Dab1 at 25°C in 50 mM Tris (pH 6.8) containing 150 mM NaCl and 0.2 mM DTT. To

calculate a dissociation constant, we plotted data and performed curve fitting with the program Origin 5.0. For fluorescence polarization measurements, a fluorescent derivative of the 14-residue ApoER2 peptide was prepared by conjugation of 5-iodoacetamidofluorescein to acetyl-CGGTKSMNFDNPVYRKT-amide (the 14-residue tail peptide extended with a CCG N-terminal linker) through a thioether linkage. After HPLC purification, the peptide was dissolved in 20 mM Na<sub>2</sub>HPO<sub>4</sub> (pH 6.8), 150 mM NaCl, and 0.2 mM DTT, and its concentration was determined by measuring the absorbance of fluorescein at 492 nm. Measurements of fluorescence anisotropy were carried out on an SLM/AMINCO AB2 luminescence spectrophotometer fitted with polarizers (Thermospectronic) at 25°C in 20 mM Na<sub>2</sub>HPO<sub>4</sub> buffer (pH 6.8) containing 150 mM NaCl and 0.2 mM DTT. Aliquots of the Dab1 PTB domain (up to a final concentration of 5 μM) were titrated into a solution of 50 nM fluorescent peptide, and the polarization value was measured. The binding curve was fit to a single site model to determine the dissociation constant. For competition measurements of fluorescence polarization with the unconjugated 14-residue peptide and the shorter 10-residue tail peptide (acetyl-NFDNPVYRKT-amide), aliquots of unconjugated peptide were added to a solution of 50 nM fluorescent peptide in the presence of 500 nM Dab1 PTB domain.

### Protein Crystallization

The purified PTB domain of mDab1 was concentrated to 15–25 mg/ml in 50 mM Tris buffer (pH 6.8) containing 50 mM NaCl and 5 mM DTT. Complexes of the PTB domain with the ApoER2 14-residue peptide were then prepared by mixing the peptide in a 1:1–1:1.5 molar ratio with protein. Initial crystals grew from 2 μl hanging drops (1 μl well solution mixed with 1 μl concentrated protein solution) after 5 weeks at room temperature in 0.1 M HEPES (pH 7.5), 20% PEG4000, and 10% isopropanol. Crystals were obtained in 2–3 days by mixing 2 μl of protein/peptide solution with 2 μl of 0.1 M HEPES (pH 7.5), 34%–36% PEG8000, and 5% ethanol over a well solution of 0.1 M HEPES (pH 7.5) and 34%–36% PEG8000 and by macroseeding 24 hr after the drops were set. Selenomethionine-derivatized crystals grew in 7–10 days under the same conditions. The crystals belong to the space group P2<sub>1</sub>2<sub>1</sub>2<sub>1</sub> and have cell dimensions of a = 36.25 Å, b = 45.72 Å, and c = 90.12 Å.

### Data Collection and Structure Determination

All diffraction data were collected at 100 K after slow transfer of the crystals into mother liquor to which 5% PEG400 had been added for cryoprotection. A native data set to 1.5 Å was collected at the Cornell High Energy Synchrotron Source (Cornell University) with the F1 beamline with an ADSC Quantum4 CCD detector. A second data set was also collected to 1.8 Å with a selenomethionine crystal from the L87M protein with a rotating anode source (Rigaku RU-200EBH) with a mar300 Image Plate Detector (mar research). Oscillation images were indexed and integrated with DENZO [39], and the intensities were scaled and merged with the program SCALEPACK [39]. The same L87M crystal was used to collect diffraction data to 2.0 Å at three wavelengths for MAD phasing at the National Synchrotron Light Source (Brookhaven National Laboratory) with the X12C beamline with a B4 CCD detector. MAD data were processed with the HKL2000 program suite [39]. The scaled intensity data from the three MAD wavelengths were input into the program SOLVE [40] to locate heavy atom sites. Two selenium sites were located, and the phases generated by SOLVE were refined with RESOLVE [40] and the program DM in the CCP4 program suite [41]. With the 1.5 Å native data set and the program ARP/wARP [42], the phases were further improved, and an atomic model (~90% complete) was built in an automatic fashion. The model was completed and manually refit with the program O [43], and simulated annealing, energy minimization, and B factor refinement were performed with CNS [44]. Further refinement included the addition of water molecules as well as a phosphate ion to the model and then further cycles of CNS refinement.

### PI-4,5P<sub>2</sub> Soaking and Ternary Complex

#### Structure Determination

Native crystals of the Dab1 PTB domain-ApoER2 peptide complex were soaked for 14 days in 50 μl of mother liquor containing 0.5

mM PI-4,5P<sub>2</sub> (Sigma). A 1.9 Å data set was collected on one of these crystals with a rotating anode source (Rigaku RU-200EBH) with a mar300 Image Plate Detector (mar research). Data were processed with DENZO and SCALEPACK as above. The amplitudes from this data set and the phases from the Dab1 PTB domain-peptide complex structure were used to generate an electron density map of the ternary complex. The map showed strong density for the phosphates in the 4 and 5 positions. The density for the inositol ring and the 1-phosphate group indicated that the PI-4,5P<sub>2</sub> adopts either of two possible orientations in the soaked crystals (see text). Occupancy refinement of these two alternate conformations assigned an occupancy of 0.7 to the preferred orientation, in which the 1-phosphate approaches within H bonding distance of the Arg76 guanidino group, and an occupancy of 0.3 to the other orientation. Simulated annealing, energy minimization, and B factor refinement were performed with CNS for both of the models. The two sets of refined PI-4,5P<sub>2</sub> coordinates were then combined into a final model with weighted occupancy, from which the 2F<sub>o</sub> - F<sub>c</sub> map of Figure 5 was generated.

#### Homology Modeling and Molecular Graphics

The models of the PTB domain from murine Disabled-2 (Dab2) and of human ARH1 were prepared with the program Modeller [45]. Figures were prepared with the programs GRASP [46], MOLSCRIPT [47], and PyMol (DeLano Scientific; <http://www.pymol.org>).

#### Acknowledgments

This research is supported by National Institutes of Health grants to S.C.B. (HL61001) and M.J.E. S.C.B. is a Pew Scholar in the Biomedical Sciences and an Established Investigator of the American Heart Association. M.J.E. is a Scholar of the Leukemia and Lymphoma Society of America. P.C.S. is an NSF predoctoral fellow, and H.J. is an AHA postdoctoral fellow. We thank Anand Saxena and the staff of the X12C beamline at BNL and the Research Resource for Macromolecular Crystallography at the National Synchrotron Light Source funded by the NIH National Center for Research Resources and the DOE Office of Biological and Environmental Research. This work is also based upon research conducted at the Cornell High Energy Synchrotron Source (CHESS), which is supported by the National Science Foundation under award DMR-9311772, with macromolecular diffraction at the CHESS (MacCHESS) facility, which is supported by award RR-01646 from the NIH. J.H. is supported by grants from the NIH (HL20948, HL63762, and NS43408), the Alzheimer Association, and the Perot Family Foundation and is the recipient of a Wolfgang-Paul Award by the Humboldt Foundation.

Received: December 30, 2002

Revised: January 31, 2003

Accepted: February 5, 2003

Published online: March 31, 2003

#### References

- Gertler, F.B., Bennett, R.L., Clark, M.J., and Hoffmann, F.M. (1989). *Drosophila* abl tyrosine kinase in embryonic CNS axons: a role in axonogenesis is revealed through dosage-sensitive interactions with disabled. *Cell* 58, 103–113.
- Gertler, F.B., Hill, K.K., Clark, M.J., and Hoffmann, F.M. (1993). Dosage-sensitive modifiers of *Drosophila* abl tyrosine kinase function: prospero, a regulator of axonal outgrowth, and disabled, a novel tyrosine kinase substrate. *Genes Dev.* 7, 441–453.
- Howell, B.W., Hawkes, R., Soriano, P., and Cooper, J.A. (1997). Neuronal position in the developing brain is regulated by mouse disabled-1. *Nature* 389, 733–737.
- Sheldon, M., Rice, D.S., D'Arcangelo, G., Yoneshima, H., Nakajima, K., Mikoshiba, K., Howell, B.W., Cooper, J.A., Goldowitz, D., and Curran, T. (1997). Scrambler and yotari disrupt the disabled gene and produce a reeler-like phenotype in mice. *Nature* 389, 730–733.
- D'Arcangelo, G., Miao, G.G., Chen, S.C., Soares, H.D., Morgan, J.I., and Curran, T. (1995). A protein related to extracellular matrix proteins deleted in the mouse mutant reeler. *Nature* 374, 719–723.
- Trommsdorff, M., Gotthardt, M., Hiesberger, T., Shelton, J., Stockinger, W., Nimpf, J., Hammer, R.E., Richardson, J.A., and Herz, J. (1999). Reeler/Disabled-like disruption of neuronal migration in knockout mice lacking the VLDL receptor and ApoE receptor 2. *Cell* 97, 689–701.
- Hiesberger, T., Trommsdorff, M., Howell, B.W., Goffinet, A., Mumby, M.C., Cooper, J.A., and Herz, J. (1999). Direct binding of Reelin to VLDL receptor and ApoE receptor 2 induces tyrosine phosphorylation of disabled-1 and modulates tau phosphorylation. *Neuron* 24, 481–489.
- D'Arcangelo, G., Homayouni, R., Keshvara, L., Rice, D.S., Sheldon, M., and Curran, T. (1999). Reelin is a ligand for lipoprotein receptors. *Neuron* 24, 471–479.
- Trommsdorff, M., Borg, J.P., Margolis, B., and Herz, J. (1998). Interaction of cytosolic adaptor proteins with neuronal apolipoprotein E receptors and the amyloid precursor protein. *J. Biol. Chem.* 273, 33556–33560.
- Gotthardt, M., Trommsdorff, M., Nevitt, M.F., Shelton, J., Richardson, J.A., Stockinger, W., Nimpf, J., and Herz, J. (2000). Interactions of the low density lipoprotein receptor gene family with cytosolic adaptor and scaffold proteins suggest diverse biological functions in cellular communication and signal transduction. *J. Biol. Chem.* 275, 25616–25624.
- Howell, B.W., Gertler, F.B., and Cooper, J.A. (1997). Mouse disabled (mDab1): a Src binding protein implicated in neuronal development. *EMBO J.* 16, 121–132.
- Blaikie, P., Immanuel, D., Wu, J., Li, N., Yajnik, V., and Margolis, B. (1994). A region in Shc distinct from the SH2 domain can bind tyrosine-phosphorylated growth factor receptors. *J. Biol. Chem.* 269, 32031–32034.
- Kavanaugh, W.M., and Williams, L.T. (1994). An alternative to SH2 domains for binding tyrosine-phosphorylated proteins. *Science* 266, 1862–1865.
- Kavanaugh, W.M., Turck, C.W., and Williams, L.T. (1995). PTB domain binding to signaling proteins through a sequence motif containing phosphotyrosine. *Science* 268, 1177–1179.
- Howell, B.W., Lanier, L.M., Frank, R., Gertler, F.B., and Cooper, J.A. (1999). The disabled 1 phosphotyrosine-binding domain binds to the internalization signals of transmembrane glycoproteins and to phospholipids. *Mol. Cell. Biol.* 19, 5179–5188.
- Harlan, J.E., Hajduk, P.J., Yoon, H.S., and Fesik, S.W. (1994). Pleckstrin homology domains bind to phosphatidylinositol 4,5-bisphosphate. *Nature* 371, 168–170.
- Hyvonen, M., Macias, M.J., Nilges, M., Oschkinat, H., Saraste, M., and Wilmanns, M. (1995). Structure of the binding site for inositol phosphates in a PH domain. *EMBO J.* 14, 4676–4685.
- Lemmon, M.A., Ferguson, K.M., Sigler, P.B., and Schlessinger, J. (1995). Specific and high-affinity binding of inositol phosphates to an isolated pleckstrin homology domain. *Proc. Natl. Acad. Sci. USA* 92, 10472–10476.
- Mishra, S.K., Keyel, P.A., Hawryluk, M.J., Agostinelli, N.R., Watkins, S.C., and Traub, L.M. (2002). Disabled-2 exhibits the properties of a cargo-selective endocytic clathrin adaptor. *EMBO J.* 21, 4915–4926.
- Zhang, Z., Lee, C.H., Mandiyan, V., Borg, J.P., Margolis, B., Schlessinger, J., and Kuriyan, J. (1997). Sequence-specific recognition of the internalization motif of the Alzheimer's amyloid precursor protein by the X11 PTB domain. *EMBO J.* 16, 6141–6150.
- Farooq, A., Plotnikova, O., Zeng, L., and Zhou, M.M. (1999). Phosphotyrosine binding domains of Shc and insulin receptor substrate 1 recognize the NPXpY motif in a thermodynamically distinct manner. *J. Biol. Chem.* 274, 6114–6121.
- Zwahlen, C., Li, S.C., Kay, L.E., Pawson, T., and Forman-Kay, J.D. (2000). Multiple modes of peptide recognition by the PTB domain of the cell fate determinant Numb. *EMBO J.* 19, 1505–1515.
- Yan, K.S., Kuti, M., Yan, S., Mujtaba, S., Farooq, A., Goldfarb, M.P., and Zhou, M.M. (2002). FRS2 PTB domain conformation regulates interactions with divergent neurotrophic receptors. *J. Biol. Chem.* 277, 17088–17094.
- Zhou, M.M., Ravichandran, K.S., Olejniczak, E.F., Petros, A.M.,

- Meadows, R.P., Sattler, M., Harlan, J.E., Wade, W.S., Burakoff, S.J., and Fesik, S.W. (1995). Structure and ligand recognition of the phosphotyrosine binding domain of Shc. *Nature* **378**, 584–592.
25. Li, S.C., Zwahlen, C., Vincent, S.J., McGlade, C.J., Kay, L.E., Pawson, T., and Forman-Kay, J.D. (1998). Structure of a Numb PTB domain-peptide complex suggests a basis for diverse binding specificity. *Nat. Struct. Biol.* **5**, 1075–1083.
26. Eck, M.J., Dhe-Paganon, S., Trub, T., Nolte, R.T., and Shoelson, S.E. (1996). Structure of the IRS-1 PTB domain bound to the juxtamembrane region of the insulin receptor. *Cell* **85**, 695–705.
27. Chang, D.D., Hoang, B.Q., Liu, J., and Springer, T.A. (2002). Molecular basis for interaction between Icap1 alpha PTB domain and beta 1 integrin. *J. Biol. Chem.* **277**, 8140–8145.
28. Beffert, U., Morfini, G., Bock, H.H., Reyna, H., Brady, S.T., and Herz, J. (2002). Reelin-mediated signaling locally regulates protein kinase B/Akt and glycogen synthase kinase 3beta. *J. Biol. Chem.* **277**, 49958–49964.
29. Bock, H.H., and Herz, J. (2003). Reelin activates SRC family tyrosine kinases in neurons. *Curr. Biol.* **13**, 18–26.
30. Xu, X.X., Yang, W., Jackowski, S., and Rock, C.O. (1995). Cloning of a novel phosphoprotein regulated by colony-stimulating factor 1 shares a domain with the *Drosophila* disabled gene product. *J. Biol. Chem.* **270**, 14184–14191.
31. He, G., Gupta, S., Yi, M., Michaely, P., Hobbs, H.H., and Cohen, J.C. (2002). ARH is a modular adaptor protein that interacts with the LDL receptor, clathrin, and AP-2. *J. Biol. Chem.* **277**, 44044–44049.
32. Mishra, S.K., Watkins, S.C., and Traub, L.M. (2002). The autosomal recessive hypercholesterolemia (ARH) protein interfaces directly with the clathrin-coat machinery. *Proc. Natl. Acad. Sci. USA* **99**, 16099–16104.
33. Ferguson, K.M., Lemmon, M.A., Schlessinger, J., and Sigler, P.B. (1995). Structure of the high affinity complex of inositol trisphosphate with a phospholipase C pleckstrin homology domain. *Cell* **83**, 1037–1046.
34. Ravichandran, K.S., Zhou, M.M., Pratt, J.C., Harlan, J.E., Walk, S.F., Fesik, S.W., and Burakoff, S.J. (1997). Evidence for a requirement for both phospholipid and phosphotyrosine binding via the Shc phosphotyrosine-binding domain in vivo. *Mol. Cell. Biol.* **17**, 5540–5549.
35. Rameh, L.E., Arvidsson, A., Carraway, K.L., III, Couvillon, A.D., Rathbun, G., Crompton, A., VanRenterghem, B., Czech, M.P., Ravichandran, K.S., Burakoff, S.J., et al. (1997). A comparative analysis of the phosphoinositide binding specificity of pleckstrin homology domains. *J. Biol. Chem.* **272**, 22059–22066.
36. Dhe-Paganon, S., Ottinger, E.A., Nolte, R.T., Eck, M.J., and Shoelson, S.E. (1999). Crystal structure of the pleckstrin homology-phosphotyrosine binding (PH-PTB) targeting region of insulin receptor substrate 1. *Proc. Natl. Acad. Sci. USA* **96**, 8378–8383.
37. Howell, B.W., Herrick, T.M., and Cooper, J.A. (1999). Reelin-induced tyrosine phosphorylation of disabled 1 during neuronal positioning. *Genes Dev.* **13**, 643–648.
38. Howell, B.W., Herrick, T.M., Hildebrand, J.D., Zhang, Y., and Cooper, J.A. (2000). Dab1 tyrosine phosphorylation sites relay positional signals during mouse brain development. *Curr. Biol.* **10**, 877–885.
39. Minor, W., Tomchick, D., and Otwinowski, Z. (2000). Strategies for macromolecular synchrotron crystallography. *Structure* **8**, R105–R110.
40. Terwilliger, T.C., and Berendzen, J. (1999). Automated MAD and MIR structure solution. *Acta Crystallogr. D Biol. Crystallogr.* **55**, 849–861.
41. Cowtan, K.D. (1994). An automated procedure for phase improvement by density modification. *Joint CCP4 and ESF-EACBM Newsletter on Protein Crystallography* **31**, 34–38.
42. Perrakis, A., Morris, R., and Lamzin, V.S. (1999). Automated protein model building combined with iterative structure refinement. *Nat. Struct. Biol.* **6**, 458–463.
43. Jones, T.A., Zou, J.-Y., Cowan, S.W., and Kjeldgaard, M. (1991). Improved methods for binding protein models in electron density maps and the location of errors in these models. *Acta Crystallogr. A* **47**, 110–119.
44. Brunger, A.T., Adams, P.D., Clore, G.M., DeLano, W.L., Gros, P., Grosse-Kunstleve, R.W., Jiang, J.S., Kuszewski, J., Nilges, M., Pannu, N.S., et al. (1998). Crystallography and NMR system: a new software suite for macromolecular structure determination. *Acta Crystallogr. D Biol. Crystallogr.* **54**, 905–921.
45. Sali, A., and Blundell, T.L. (1993). Comparative protein modelling by satisfaction of spatial restraints. *J. Mol. Biol.* **234**, 779–815.
46. Nicholls, A., Sharp, K., and Honig, B. (1991). Protein folding and association: insights from the interfacial and thermodynamic properties of hydrocarbons. *Proteins Struct. Funct. Genet.* **11**, 281–296.
47. Kraulis, P. (1991). MOLSCRIPT: a program to produce both detailed and schematic plots of protein structures. *J. Appl. Crystallogr.* **24**, 946–950.

#### Accession Numbers

Coordinates for the PTB domain-ApoER2 complex have been deposited in the Protein Data Bank under accession number 1NTV; coordinates for the complex with bound PI-4,5P<sub>2</sub> have been deposited in the Protein Data Bank under accession number 1NU2.